An End-To-End Intelligent EEG Bad Channel Detection and Reconstruction System Using Deep Learning and Reservoir Computing

1st Zhaojin Chen
School of Computer Science, Beijing University of Technology
Beijing Key Laboratory of Trusted Computing
National Engineering Laboratory for Key Technologies of Information Security Level Protection
Beijing, China
chenzhaojin2001@163.com

2nd Lijuan Duan
School of Computer Science, Beijing University of Technology
Beijing Key Laboratory of Trusted Computing
National Engineering Laboratory for Key Technologies of Information Security Level Protection
Beijing, China
ljduan@bjut.edu.cn (Corresponding Author)

3rd Changming Wang
Luhe Hospital, Capital Medical University
College of Biomedical Engineering, Capital Medical University
Jingtong Brain Research Laboratory
Beijing, China
superwcm@gmail.com (Corresponding Author)

4th Xixi Zhao
Anding Hospital, Capital Medical University
Beijing, China
zhaoxixi@ccmu.edu.cn

5th Zijian Zhou
School of Psychology and Mental Health, North China University of Science and Technology
Hebei, China
15233259087@163.com

Abstract—Bad channels significantly compromise EEG analysis, yet existing solutions often struggle with generalization or rely on precise electrode coordinates that are frequently unavailable. This study proposes an automated framework that integrates deep learning and reservoir computing without requiring electrode coordinates. The system features a Bad Channel Long Short-Term Memory (BC-LSTM) network with multi-order differential features for precise anomaly detection, and a Correlation-Weighted Reservoir Computing (CWRC) module for signal reconstruction. We also introduce a detection-guided data selection strategy to ensure artifact-free training, alongside a Neural Electrophysiological Similarity-Driven Transfer Learning (NESTL) mechanism to address data scarcity. Experimental results across 19-, 32-, and 64-channel datasets demonstrate 92.4% detection accuracy and an 80% improvement in reconstruction quality over traditional interpolation. The proposed system provides an effective automated solution for EEG preprocessing, suitable for both clinical and research applications.

Index Terms—EEG, LSTM, Reservoir Computing, Transfer learning, Bad Channel

I. Introduction

Electroencephalography (EEG) is widely used in neuroscience and clinical diagnostics due to its millisecond-level temporal resolution, portability, and cost-effectiveness [1]. In practical, EEG applications face significant challenges from "bad channels"—electrodes that fail to capture valid neuronal activity due to high impedance, connection failures, or amplifier malfunctions. As illustrated in Fig. 1, these channels exhibit high-amplitude noise, saturation, or silence. Such anomalies not only result in information loss but also disrupt downstream analyses: they severely compromise preprocessing algorithms like Independent Component Analysis (ICA) and Artifact Subspace Reconstruction (ASR) [2], [3], distort source localization by altering spatial topologies [4], and degrade the performance of machine learning models [5].

Given these challenges, effective bad channel detection and reconstruction are essential. Traditional approaches typically involve manual detection, which is subjective and labor-intensive, or automated statistical methods [6], [7]

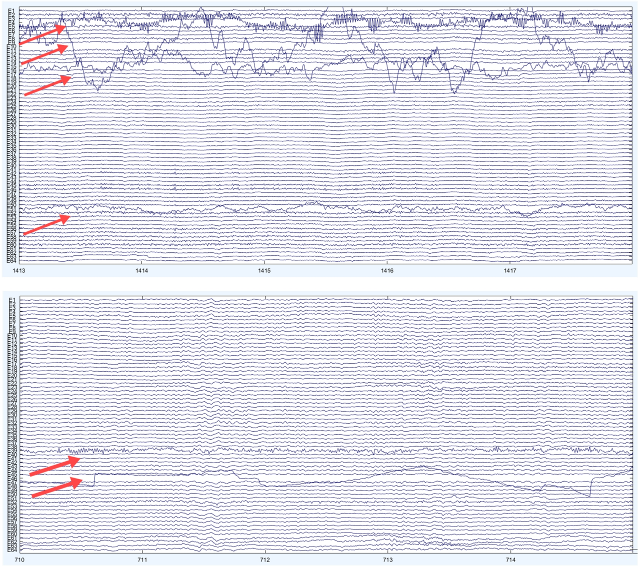

Fig. 1: Illustration of common bad channel artifacts in EEG recordings.

that often struggle to generalize across variable experimental conditions. For signal recovery, standard interpolation techniques (e.g., spherical spline) rely heavily on static spatial relationships and precise electrode coordinates [8], [9]. These methods fail to capture temporal dynamics and suffer significant accuracy loss when coordinate information is missing or inaccurate—a common issue in practical scenarios. While deep learning offers new avenues, specifically Long Short-Term Memory (LSTM) networks for temporal feature learning [10] and Reservoir Computing (RC) for efficient signal reconstruction [11], [12], existing implementations often require ideal, noise-free training data [13], a condition rarely met in clinical reality.

To address these limitations, this research proposes an integrated, fully automated EEG bad channel processing system. Our approach combines an improved LSTM network (BC-LSTM) for robust detection with a Correlation-Weighted Reservoir Computing (CWRC) framework for adaptive reconstruction. Unlike traditional methods dependent on spatial coordinates, our system leverages temporal dynamics and intrinsic signal correlations to perform robustly even without explicit electrode position information.

We introduce four primary innovations:

1) Adaptive BC-LSTM Architecture: An improved LSTM that combines raw signals with differential features and uses a dynamic weight adjustment mechanism to handle the non-stationary nature of EEG signals.
2) Coordinate-Free Reconstruction: A graph embedding-based correlation weight matrix that optimizes reconstruction weights without requiring explicit electrode position information.
3) High-Quality Data Selection: A strategy to automatically identify valid training segments with high signal-to-noise ratios, preventing the contamination of the RC model by artifacts.
4) Neural Electrophysiological Similarity-Driven Transfer Learning (NESTL): A method to address data scarcity by leveraging reconstruction models from subjects with similar electrophysiological profiles.

Systematic evaluation on 19, 32, and 64-channel datasets demonstrates that this system significantly outperforms traditional detection and interpolation methods. By effectively managing multiple co-existing bad channels and operating independently of electrode coordinates, this work provides a reliable foundation for high-quality EEG analysis in both research and clinical settings.

II. Related Work

A. Bad Channel Detection

Bad channel detection methods primarily fall into statistical and machine learning categories. Widely used artifact removal pipelines, such as FASTER and HAPPE, employ statistical thresholding to identify bad channels [6], [14]. Iterative approaches like the Iterative Standard Deviation (ISD) method [15] improve detection but require sensitive hyperparameter tuning. More recently, unsupervised learning methods such as the Local Outlier Factor (LOF) [16] and deep learning approaches like cleanEEGNet (a 2D-CNN) [17] have demonstrated superior performance over traditional statistical baselines. These methods require fixed input dimensions or substantial annotated data, limiting their flexibility in dynamic clinical environments.

B. Bad Channel Reconstruction

Traditional reconstruction relies on interpolation, which depends heavily on precise electrode coordinates. Recent deep learning advancements have introduced data-driven alternatives. Methods utilizing spatiotemporal correlation [18] and deep autoencoders [19] have shown promise in self-supervised reconstruction. Generative models, including WGAN-based approaches [20] and convolution-based upsampling [21], can generate realistic EEG signals even with reduced electrode counts. The EC-informer model [22] further improved efficiency in cross-subject transfer. Despite these advances, most deep learning models struggle when multiple adjacent channels fail simultaneously or when training data distributions diverge significantly from test data due to inter-subject variability.

C. Reservoir Computing in EEG

RC has gained traction in EEG analysis due to its computational efficiency and ability to model non-linear temporal dynamics [23]. It has been successfully applied to epileptic seizure prediction [24] and extensively used in emotion recognition tasks, handling variations across

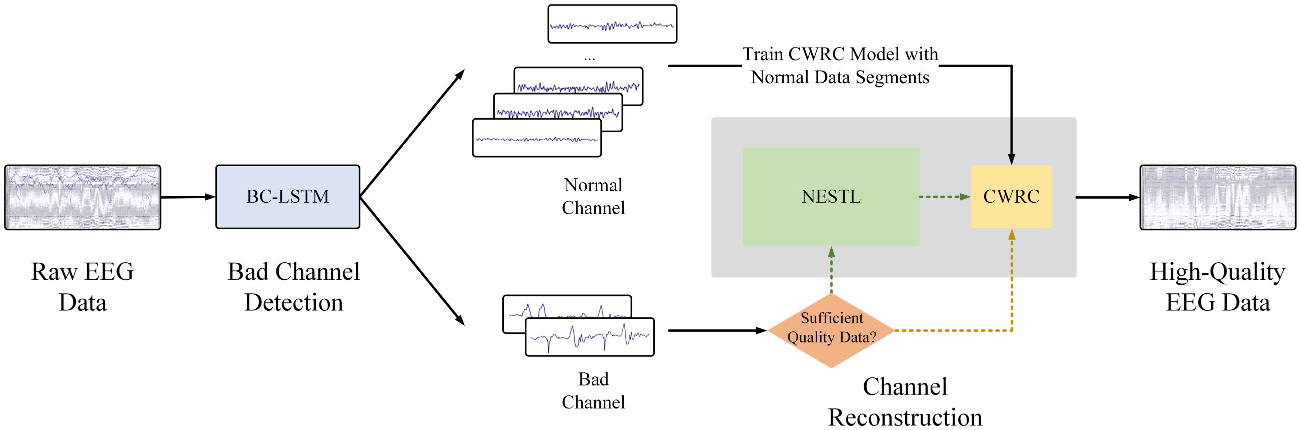

Fig. 2: Overview of the proposed system architecture.

trials and subjects [12], [25]–[27]. Additionally, RC combined with transfer learning has shown robust pattern recognition capabilities [28].

Relevant to this study, RC has been investigated for hidden data recovery. Previous work demonstrated that RC outperforms linear interpolation in reconstructing missing EEG signals [13]. That approach assumed the availability of ideal, noise-free periods for training the readout layer—an assumption rarely met in real-world clinical data. This research addresses that gap by introducing a robust selection and weighting mechanism that eliminates the need for pristine ground-truth data.

III. Method

A. System Architecture Overview

We propose an integrated framework for EEG bad channel detection and reconstruction (Fig. 2), consisting of a detection module and a reconstruction module.

EEG signals are segmented into fixed-length windows and processed by a BC-LSTM to detect abnormal segments. Channels are classified as good or bad based on the proportion and temporal continuity of detected abnormalities, enabling separation of transient artifacts from persistently corrupted channels.

For reconstruction, if a bad channel contains sufficient normal segments, a subject-specific CWRC model is trained. It employs a signal-driven correlation weighting mechanism to adaptively fuse information from remaining channels without requiring electrode position information.

When normal segments are unavailable, NESTL is applied. This strategy selects a similar subject and transfers the corresponding CWRC model to reconstruct the target bad channel. In cases with multiple bad channels, only identified good channels are used as reconstruction inputs. Finally, reconstructed signals are combined with original good channels to produce complete EEG recordings.

B. Bad Channel Detection Module

EEG bad channel detection is challenging due to diverse abnormal patterns, including amplitude outliers, rapid oscillations, and slow drifts. To capture these heterogeneous characteristics, we construct multi-order differential representations. Given a signal segment $\mathbf{s} \in \mathbb{R}^W$, its first- and second-order differences are computed and stacked with the original signal to form a three-channel input $\mathbf{X} \in \mathbb{R}^{3\times W}$, enabling complementary descriptions of signal magnitude, rate of change, and acceleration.

To adaptively emphasize informative components, we propose a BC-LSTM with dynamic input reweighting. The key intuition is that different bad channel types manifest distinct temporal behaviors. Therefore, the relative importance of the original signal and its differential components should vary over time.

Let $\mathbf{c}_t$ denote the LSTM cell state at time t. BC-LSTM leverages the previous cell state $\mathbf{c}_{t-1}$, which summarizes the current waveform context, to generate adaptive weights for the input at the next time step:

$$\tilde{\mathbf{x}}_t = \mathbf{x}_t \odot \sigma(\mathrm{conv}(\mathbf{c}_{t-1})), \tag{1}$$

where $\mathbf{x}_t \in \mathbb{R}^3$ is the three-channel input at time t, $\odot$ denotes element-wise multiplication, $\mathrm{conv}(\cdot)$ maps $\mathbf{c}_{t-1}$ to a 3-dimensional weight vector, and $\sigma(\cdot)$ is the sigmoid function. The remaining LSTM state updates follow the standard formulation.

C. Bad Channel Reconstruction Module

The reconstruction module recovers signals from identified bad channels using information from remaining good channels. We consider two scenarios: subject-specific reconstruction, where sufficient normal segments exist, and transfer learning-based reconstruction, where data is scarce.

To capture nonlinear inter-channel relationships, we adopt the CWRC framework, which enhances standard RC by introducing a signal-driven correlation weighting mechanism that adaptively modulates the contribution of each input channel.

1) RC-based Reconstruction: Reconstruction is performed channel-wise. For each bad channel, we use n good channels as input to reconstruct a single target signal. Before entering the reservoir, input signals are modulated by a correlation weight matrix:

$$\mathbf{X}_{\mathrm{w}} = \mathbf{W}_{\mathrm{corr}} \cdot \mathbf{X}_{\mathrm{origin}}, \tag{2}$$

where $\mathbf{X}_{\mathrm{origin}} \in \mathbb{R}^{n\times T}$ denotes the original input signals from n good channels, and $\mathbf{W}_{\mathrm{corr}} \in \mathbb{R}^{n\times n}$ is a diagonal weight matrix adjusting channel contributions.

The reservoir state is updated according to:

$$\mathbf{r}_{t+1} = (1 - l_r)\mathbf{r}_t + l_r \tanh(\mathbf{W}_{\mathrm{res}}\mathbf{r}_t + \mathbf{W}_{\mathrm{in}}\mathbf{x}_{\mathrm{w},t}), \tag{3}$$

where $\mathbf{r}_t \in \mathbb{R}^{N_r}$ is the reservoir state at time t, $\mathbf{x}_{\mathrm{w},t}$ is the t-th column of $\mathbf{X}_{\mathrm{w}}$, $\mathbf{W}_{\mathrm{res}} \in \mathbb{R}^{N_r\times N_r}$ and $\mathbf{W}_{\mathrm{in}} \in \mathbb{R}^{N_r\times n}$ are fixed internal and input weight matrices, and l_r is the leakage rate.

The reconstructed signal is obtained via a linear readout:

$$y_t = \mathbf{W}_{\mathrm{out}}\mathbf{r}_t, \tag{4}$$

where $\mathbf{W}_{\mathrm{out}} \in \mathbb{R}^{1\times N_r}$ is trained using ridge regression. Let $\mathbf{R} = [\mathbf{r}_1, \dots, \mathbf{r}_T] \in \mathbb{R}^{N_r\times T}$ and $\mathbf{y} = [y_1, \dots, y_T]$, then:

$$\mathbf{W}_{\mathrm{out}} = \mathbf{y}\mathbf{R}^{\mathsf{T}}(\mathbf{R}\mathbf{R}^{\mathsf{T}} + \eta\mathbf{I})^{-1}. \tag{5}$$

2) Graph Embedding-based Correlation Weight Matrix: To address the limitations of spatial interpolation, we construct a signal-driven correlation weight matrix based on functional relationships. Given input $\mathbf{X}_{\mathrm{origin}} \in \mathbb{R}^{n\times T}$, we first compute the Pearson correlation matrix $\mathbf{R}_{\mathrm{corr}} \in \mathbb{R}^{n\times n}$ among input channels. The adjacency matrix $\mathbf{A}$ is constructed as:

$$A_{ij} = |(\mathbf{R}_{\mathrm{corr}})_{ij}|, \quad A_{ii} = 0. \tag{6}$$

The normalized graph Laplacian is computed as:

$$\mathbf{L}_{\mathrm{norm}} = \mathbf{D}^{-\frac{1}{2}}(\mathbf{D} - \mathbf{A})\mathbf{D}^{-\frac{1}{2}}, \tag{7}$$

where $\mathbf{D}$ is the degree matrix with $D_{ii} = \sum_j A_{ij}$.

Eigen-decomposition of $\mathbf{L}_{\mathrm{norm}}$ yields an embedding matrix $\mathbf{E} \in \mathbb{R}^{n\times k}$. The correlation weight for input channel i is:

$$w_i = \gamma + \alpha\left(|r_{i,\mathrm{target}}| - \beta\sum_{j=1}^{k} E_{i,j}^2\right), \tag{8}$$

where $r_{i,\mathrm{target}}$ is the Pearson correlation between input channel i and the target bad channel, and γ, α, β are hyperparameters. The weight matrix is then $\mathbf{W}_{\mathrm{corr}} = \mathrm{diag}(w_1, \dots, w_n)$.

Algorithm 1 NESTL-based Cross-Subject Reconstruction

Require: Dataset $\mathcal{D}$, target subject S_t, bad channel c_b, parameter K
Ensure: Reconstructed signal $\hat{y}_{c_b}$

```
Screen eligible candidate subjects S from D
Select simulated bad channel c_sim from S_t
Stage 1: Similarity assessment
for each candidate S_i ∈ S do
    Train CWRC model M_i^sim on S_i to reconstruct c_sim
    Apply M_i^sim to S_t to obtain ŷ_sim
    Compute error e_i = MSE(c_sim, ŷ_sim)
end for
Stage 2: Model transfer
S_top ← top-K candidates with lowest e_i
Randomly select S_sel from S_top
Train CWRC model M_sel on S_sel to reconstruct c_b
Apply M_sel to S_t to obtain ŷ_{c_b}
return ŷ_{c_b}
```

3) Neural Electrophysiological Similarity-Driven Transfer Learning: When subject-specific data is insufficient, NESTL transfers models from similar subjects. A proxy-based similarity evaluation is used: a known good channel (e.g., Cz) in the target subject is treated as a simulated bad channel to evaluate how well models from candidate subjects can reconstruct it. The process is detailed in Algorithm 1.

Here, $\mathcal{S}$ denotes the set of eligible candidate subjects, S_i is the i-th candidate, M_i^{sim} is the CWRC model trained on S_i for reconstructing the simulated channel, $\hat{y}_{\mathrm{sim}}$ is the predicted signal for c_{sim}, $\mathcal{S}_{\mathrm{top}}$ contains the top-K candidates with lowest errors, S_{sel} is the randomly selected candidate, and M_{sel} is the final CWRC model used for reconstruction.

IV. Experiment

A. Datasets

Three EEG datasets with different electrode configurations were used for evaluation.

DEAP dataset [29]: A public dataset containing EEG recordings from 32 subjects during emotion elicitation experiments, collected using a 32-channel system following the international 10-20 standard.

19-channel private dataset: EEG data collected using a face-building matching paradigm, including recordings from 53 schizophrenia patients and 31 healthy controls. The electrode configuration follows the international 10-20 system, and bad channels were annotated by clinical experts.

64-channel private dataset: EEG data collected using EGI equipment with 64 channels under a dot-probe paradigm, including recordings from 231 Alzheimer's disease patients. Bad channels were annotated by clinical experts.

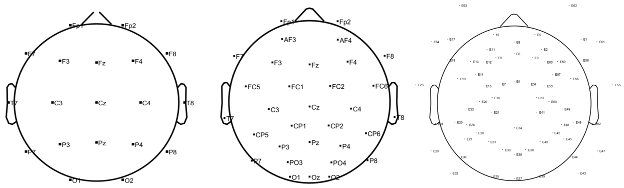

Fig. 3: Electrode layouts for the three datasets.

TABLE I: Performance Comparison of Detection Methods

Method	ACC (%)	Pre (%)	Rec (%)	F1-score (%)
Faster	58.90	70.43	50.75	58.99
HAPPE	63.25	61.59	74.39	67.39
cleanEEGNet	73.32	71.78	75.76	73.71
Ours	92.40	92.51	92.14	92.32

For both private datasets, bad channel annotations were provided by a senior clinical neurophysiologist with over 10 years of experience. Channels were labeled as bad based on persistent abnormal amplitudes or dominant abnormal segments throughout the recording. Based on these annotations, abnormal segments from bad channels and normal segments from good channels were randomly sampled to form balanced positive and negative samples for detection tasks.

Electrode layouts for all datasets are illustrated in Fig. 3. All EEG data were resampled to 250 Hz and bandpass filtered between 0.5–30 Hz. The datasets are referred to as Dataset-19CH, Dataset-32CH, and Dataset-64CH according to the number of channels.

B. Evaluation Metrics

1) Bad Channel Detection Metrics: Detection performance was evaluated using Accuracy (ACC), Precision, Recall, and F1-score:

$$\text{ACC} = \frac{TP + TN}{TP + TN + FP + FN}, \tag{9}$$

$$\text{Precision} = \frac{TP}{TP + FP}, \quad \text{Recall} = \frac{TP}{TP + FN}, \tag{10}$$

$$\text{F1} = 2 \cdot \frac{\text{Precision} \cdot \text{Recall}}{\text{Precision} + \text{Recall}}, \tag{11}$$

where TP, TN, FP, and FN denote true positives, true negatives, false positives, and false negatives, respectively.

2) Bad Channel Reconstruction Metrics: Reconstruction performance was evaluated using multiple quantitative and qualitative metrics.

MAE and MSE measure absolute and squared reconstruction errors:

$$\text{MAE} = \frac{1}{N}\sum_{i=1}^{N} |Y_i^{\text{rec}} - Y_i|, \quad \text{MSE} = \frac{1}{N}\sum_{i=1}^{N} (Y_i^{\text{rec}} - Y_i)^2. \tag{12}$$

Relative Error was adopted to normalize reconstruction errors across channels with different amplitudes:

$$\text{Relative Error} = \frac{\text{Error}(Y^{\text{rec}}, Y)}{\text{Self Error}}, \tag{13}$$

where Error($\cdot$) and Self Error are defined following standard normalized error formulations.

Pearson Correlation Coefficient (PCC) was used to assess waveform similarity:

$$\text{PCC} = \frac{\sum_i (Y_i^{\text{rec}} - \overline{Y^{\text{rec}}})(Y_i - \overline{Y})}{\sqrt{\sum_i (Y_i^{\text{rec}} - \overline{Y^{\text{rec}}})^2}\sqrt{\sum_i (Y_i - \overline{Y})^2}}. \tag{14}$$

In addition, expert visual assessment was conducted by a senior clinical neurophysiologist, who blindly scored reconstructed signals (1–5) based on waveform morphology and artifact suppression.

V. Experimental Results

A. Bad Channel Detection Performance

We first evaluate the effectiveness of the proposed detection module. We compare our BC-LSTM with Faster, HAPPE (traditional methods) [6], [14], and cleanEEGNet (CNN-based method) [17]. Testing was conducted on a combined dataset of Dataset-19CH and Dataset-64CH.

The performance comparison is detailed in Table I. As shown, Faster and HAPPE achieved accuracy rates of only 58.9% and 63.25%, respectively. cleanEEGNet showed improvement but remained inadequate for precise clinical needs. Our method achieved the highest performance across all metrics, with an accuracy of 92.4% and an F1-score of 92.32%, demonstrating its superiority in identifying abnormal channels.

B. Reconstruction Performance Evaluation

This section assesses the reconstruction quality of the proposed CWRC framework. We benchmark against Spherical Spline Interpolation (standard in EEGLAB), RC, and deep learning methods (GAN, Transformer) on Dataset-32CH.

Quantitative results are presented in Table II. The proposed CWRC method consistently outperforms the baseline RC and traditional interpolation methods across all datasets. On the DEAP dataset (Dataset-32CH), CWRC significantly reduced the Mean Squared Error (MSE) to 64.1, compared to 306.1 for Interpolation and 77.4 for basic RC.

Deep learning models (GAN and Transformer) performed poorly in this context, failing to surpass even the traditional interpolation baseline in terms of correlation coefficient. This underperformance is attributed to the fixed input dimensions of deep models, which struggle to adapt to the dynamic nature of bad channel configurations. In contrast, our reservoir-based approach offers superior flexibility.

Fig. 4 provides a visual comparison on the representative Dataset-32CH. Interpolation methods often produce

TABLE II: Quantitative Reconstruction Performance Comparison Across Datasets

Dataset	Method	Rel. Error	MAE	MSE	Corr. Coeff.	Expert Score
Dataset-19CH	Interpolation	0.1855	3.87	91.4	0.742	3.78
	RC	0.0722	3.57	55.7	0.812	4.14
	CWRC (Ours)	0.0699	3.49	51.8	0.833	4.19
Dataset-32CH	Interpolation	0.5239	7.53	306.1	0.574	3.89
	GAN	0.4145	6.73	248.8	0.665	3.21
	Transformer	0.7389	10.18	460.7	0.407	2.55
	RC	0.1250	4.27	77.4	0.879	4.33
	CWRC (Ours)	0.1002	3.97	64.1	0.891	4.41
Dataset-64CH	Interpolation	0.1642	7.81	211.0	0.720	4.23
	RC	0.0874	7.67	166.9	0.851	4.45
	CWRC (Ours)	0.0789	7.23	154.0	0.870	4.49

Note: Statistical significance assessed via Wilcoxon signed-rank tests ($p < 0.001$ for CWRC vs. Interpolation/RC on Dataset-32CH).

smoothed waveforms that miss high-frequency details or introduce unnatural artifacts. CWRC effectively reconstructs the signal by leveraging the correlation-weighted contributions from valid channels, resulting in waveforms that most closely resemble the ground truth.

C. Impact of Training Data Size

We analyzed the relationship between training data quantity and reconstruction quality (Fig. 5). While RC-based methods require a "warm-up" period, they begin to outperform interpolation once the training set exceeds approximately 300 data points. CWRC shows lower error than basic RC when data is scarce, highlighting the efficacy of the correlation weight mechanism in low-resource regimes. For practical deployment, a threshold of 600 points ensures robust performance.

D. Neural Electrophysiological Similarity-driven Transfer

Finally, we validate the NESTL strategy for scenarios where target subject data is unavailable. We tested whether selecting source models based on channel similarity improves reconstruction compared to random selection.

As illustrated in Fig. 6, we performed pairwise testing across all channel pairs. The results reveal a systematic pattern of effective transfer: consistently positive improvement trends were observed in over 84% of channel pairs across different K settings. This confirms that selecting training data based on electrophysiological similarity yields significantly better reconstruction than random selection, enabling the system to handle cold-start scenarios effectively.

VI. Conclusion and Future Work

In this paper, we presented a novel end-to-end intelligent EEG bad channel detection and reconstruction system. By integrating the proposed BC-LSTM detection module with a CWRC reconstruction framework, our approach enables fully automated processing without relying on explicit electrode position information.

Comprehensive experiments on 19-, 32-, and 64-channel datasets demonstrate the superiority of the proposed method, with BC-LSTM achieving 92.4% detection accuracy and CWRC improving reconstruction quality by up to 80% compared to traditional interpolation. Regarding computational efficiency, our system achieves a Real-Time Factor (RTF) of approximately 0.004, processing a 40-minute EEG recording in under 10 seconds. This speed, approximately 250× faster than real-time, ensures the feasibility of handling large-scale datasets in clinical research.

A key finding from our study is that the RC model can achieve robust reconstruction with as little as a few seconds of high-quality training data. This implies that ensuring a brief initial period of clean signals during acquisition could substantially reduce data loss in prolonged monitoring sessions.

Future work will focus on two main directions. First, we plan to develop a hierarchical RC framework that builds dedicated models for different functional brain regions (e.g., frontal, temporal) to capture region-specific neurophysiological characteristics. Second, we aim to optimize the channel selection strategy in the NESTL module to reduce computational overhead and further enhance transfer learning efficiency. Future work will explore applying this framework to other multi-channel signals such as multi-lead ECG.

References

[1] M. X. Cohen, "Where does EEG come from and what does it mean?" Trends in neurosciences, vol. 40, no. 4, pp. 208–218, 2017.

[2] C. B. Gonsisko, D. P. Ferris, and R. J. Downey, "iCanClean improves independent component analysis of mobile brain imaging with EEG," Sensors, vol. 23, no. 2, p. 928, 2023.

[3] R. Somervail, J. Cataldi, A. M. Stephan, V. Noreika, and T. Correia, "Dusk2dawn: an EEGLAB plugin for automatic cleaning of whole-night sleep electroencephalogram using Artifact Subspace Reconstruction," Sleep, vol. 46, no. 12, p. zsad208, 2023.

[4] V. P. Kumaravel, M. Buiatti, E. Parise, and E. Farella, "Adaptable and robust EEG bad channel detection using local outlier factor (LOF)," Sensors, vol. 22, no. 19, p. 7314, 2022.

[5] H. Cui, C. Li, A. Liu, R. Qian, and X. Chen, "A dual-branch interactive fusion network to remove artifacts from single-channel EEG," IEEE Transactions on Instrumentation and Measurement, vol. 73, pp. 1–12, 2023.

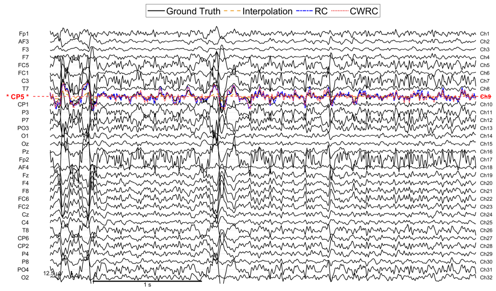

(a) Reconstruction Overview (Dataset-32CH)

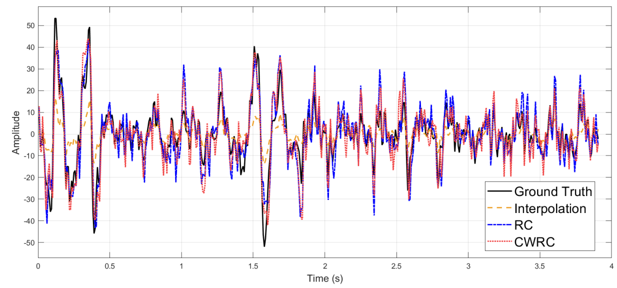

(b) Detailed Comparison (Dataset-32CH)

Fig. 4: Visual comparison of reconstruction performance on the DEAP dataset (32-Channel). (a) Displays the reconstructed signal within the complete EEG recording context. (b) Offers a zoomed-in comparison showing that CWRC (Red) most closely follows the Ground Truth (Black).

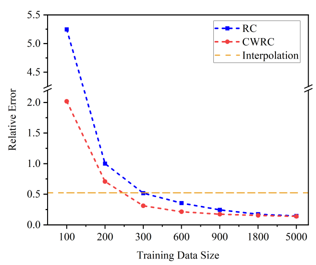

(a) Relative Error (32CH)

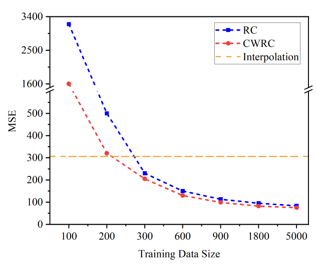

(b) MSE (32CH)

Fig. 5: Impact of training data size on reconstruction performance on Dataset-32CH.

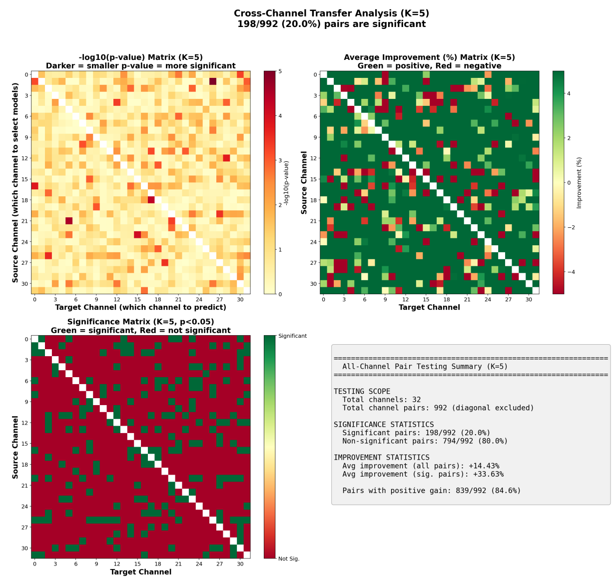

Fig. 6: Cross-channel transfer validation ($K = 5$). The matrices indicate widespread statistical significance (green), confirming that similarity-based transfer outperforms random selection.

[6] H. Nolan, R. Whelan, and R. B. Reilly, "FASTER: Fully automated statistical thresholding for EEG artifact rejection," Journal of Neuroscience Methods, vol. 192, no. 1, pp. 152–162, 2010.

[7] H. P. Kriegel, P. Kröger, E. Schubert, and A. Zimek, "LoOP: local outlier probabilities," in Proceedings of the 18th ACM conference on Information and knowledge management, 2009, pp. 1649–1652.

[8] A. C. Soong, J. C. Lind, G. R. Shaw, and Z. J. Koles, "Systematic comparisons of interpolation techniques in topographic brain mapping," Electroencephalography and clinical Neurophysiology, vol. 87, no. 4, pp. 185–195, 1993.

[9] D. Shepard, "A two-dimensional interpolation function for irregularly-spaced data," in Proceedings of the 1968 23rd ACM National Conference, 1968, pp. 517–524.

[10] S. Hochreiter, "Long Short-term Memory," Neural Computation, vol. 9, no. 8, pp. 1735–1780, 1997.

[11] M. Yan, C. Huang, P. Bienstman, P. Tino, W. Lin, and J. Sun, "Emerging opportunities and challenges for the future of reservoir computing," Nature Communications, vol. 15, no. 1, p. 2056, 2024.

[12] L. Bozhkov, P. Koprinkova-Hristova, and P. Georgieva, "Learning to decode human emotions with Echo State Networks," Neural Networks, vol. 78, pp. 112–119, 2016.

[13] A. Badarin, A. Andreev, V. Klinshov, V. Antipov, and A. E. Hramov, "Hidden data recovery using reservoir computing: Adaptive network model and experimental brain signals," Chaos: An Interdisciplinary Journal of Nonlinear Science, vol. 34, no. 10, p. 103126, 2024.

[14] L. Gabard-Durnam, A. Mendez Leal, C. Wilkinson, and A. Levin, "The Harvard Automated Processing Pipeline for Electroencephalography (HAPPE): Standardized processing software for developmental and high-artifact data," Frontiers in Neuroscience, vol. 12, p. 97, 2018.

[15] M. Komosar, P. Fiedler, and J. Haueisen, "Bad channel detection in EEG recordings," in Current Directions in Biomedical Engineering, vol. 8, no. 2. De Gruyter, 2022, pp. 257–260.

[16] M. M. Breunig, H. P. Kriegel, R. T. Ng, and J. Sander, "LOF:

identifying density-based local outliers," in Proceedings of the 2000 ACM SIGMOD international conference on Management of data, 2000, pp. 93–104.

[17] V. Kumaravel, F. Paissan, and E. Farella, "Towards a domain-specific neural network approach for EEG bad channel detection," in 2021 IEEE Signal Processing in Medicine and Biology Symposium (SPMB). IEEE, 2021, pp. 1–4.

[18] N. Bahador, J. Jokelainen, S. Mustola, and J. Kortelainen, "Reconstruction of missing channel in electroencephalogram using spatiotemporal correlation-based averaging," Journal of Neural Engineering, vol. 18, no. 5, p. 056045, 2021.

[19] S. Saba-Sadiya, T. Alhanai, T. Liu, and M. M. Ghassemi, "EEG channel interpolation using deep encoder-decoder networks," in 2020 IEEE International Conference on Bioinformatics and Biomedicine (BIBM). IEEE, 2020, pp. 2432–2439.

[20] L. L. Li, G. Z. Cao, H. J. Liang, J. C. Chen, and Y. P. Zhang, "EEG generation of virtual channels using an improved Wasserstein generative adversarial networks," in International Conference on Intelligent Robotics and Applications. Springer, 2022, pp. 386–399.

[21] M. Svantesson, H. Olausson, A. Eklund, and M. Thordstein, "Virtual EEG-electrodes: Convolutional neural networks as a method for upsampling or restoring channels," Journal of Neuroscience Methods, vol. 355, p. 109126, 2021.

[22] H. Sun, C. Li, and H. Zhang, "Design of virtual BCI channels based on informer," Frontiers in Human Neuroscience, vol. 17, p. 1150316, 2023.

[23] M. R. Hossain, N. X. Armendarez, A. S. Mohamed, A. Dhungel, J. S. Najem, and M. S. Hasan, "EEG signal classification using memristor-based reservoir computing system," in 2023 IEEE 16th Dallas Circuits and Systems Conference (DCAS). IEEE, 2023, pp. 1–4.

[24] S. Kawaguchi, A. Banerjee, J. Hirotani, and T. Tsuchiya, "MEMS resonator-based reservoir computing for epileptic seizure prediction," in 2024 IEEE International Meeting for Future of Electron Devices, Kansai (IMFEDK). IEEE, 2024, pp. 1–2.

[25] Anubhav and K. Fujiwara, "Across trials vs subjects vs contexts: A multi-reservoir computing approach for EEG variations in emotion recognition," in Proceedings of the 26th International Conference on Multimodal Interaction, 2024, pp. 518–525.

[26] R. Fourati, B. Ammar, J. Sanchez-Medina, and A. M. Alimi, "Unsupervised learning in reservoir computing for EEG-based emotion recognition," IEEE Transactions on Affective Computing, vol. 13, no. 2, pp. 972–984, 2020.

[27] J. Li, X. Wu, Y. Zhang, H. Yang, and X. Wu, "DRS-Net: A spatial–temporal affective computing model based on multichannel EEG data," Biomedical Signal Processing and Control, vol. 76, p. 103660, 2022.

[28] X. Wu, Y. Feng, S. Lou, H. Zheng, B. Hu, Z. Hong, and J. Tan, "Improving NeuCube spiking neural network for EEG-based pattern recognition using transfer learning," Neurocomputing, vol. 529, pp. 222–235, 2023.

[29] S. Koelstra, C. Muhl, M. Soleymani, J. S. Lee, A. Yazdani, T. Ebrahimi, T. Pun, A. Nijholt, and I. Patras, "DEAP: A database for emotion analysis using physiological signals," IEEE Transactions on Affective Computing, vol. 3, pp. 18–31, 2012.